2011 International Symposium on Nonlinear Theory and its Applications
NOLTA2011, Kobe, Japan, September 4-7, 2011

Nonlinear oscillations in two coupled elastic beams with tunable nonlinear potentials

Masayuki Kimura† and Takashi Hikihara‡

†School of Engineering, The University of Shiga Prefecture
2500 Hassaka-cho, Hikone, Shiga 522-8533 Japan
‡Department of Electric Engineering, Kyoto University
Katsura, Nishikyo-ku, Kyoto 615-8510 Japan
Email: kimura.m@e.usp.ac.jp, hikihara@kuee.kyoto-u.ac.jp

Abstract—Spatially localized and temporally periodic solutions exist in a nonlinear coupled oscillator arrays. Because the energy of the solution is localized within a few sites, localized solutions exist even in a two-degree-of-freedom system. In this paper, bifurcations regarding the localized solutions are investigated by using the simple averaging method. Bifurcation sets are derived analytically and it is confirmed numerically.

1. Introduction

In micro-/nano-engineering, spatially periodic structures are easily fabricated and often used to realize some novel functions. Those are often modeled as coupled oscillators array, namely, coupled ordinary differential equations. As the scale of devises decreases, the magnitude of deflection should be relatively large because the thermal fluctuation tends to be comparable with the size of the structures. Therefore, nonlinearity becomes remarkable especially in nano-scale structures.

Intrinsic localized mode (ILM) is known as a spatially localized and temporally periodic solution in nonlinear coupled oscillator arrays, which was first discovered by A. J. Sievers and S. Takeno in 1988 [1]. In this decade, it has been reported that observation and manipulation on ILM in experiments [2]. A micro-cantilever array is one of which ILM is observed and manipulated [3, 4]. The cantilever array is modeled as a nonlinear coupled ordinary equations. By using the model, we revealed the mechanism of traveling of ILM and proposed manipulation methods [5].

A macro-mechanical cantilever array is fabricated for experimental studies on ILM [6]. The macro-cantilever array is also derived by a coupled ordinary differential equations. Existence of standing ILM which is pinned at a site of array is already confirmed in both experimentally and numerically. However, a lot of things such as bifurcations or global phase structure is not clarified. This paper aims to clarify the dependence property of bifurcations of localized solutions on the linear coupling coefficient in a two-degree-of-freedom system.

2. Two coupled oscillator

Two cantilevers which are coupled each other are schematically shown in Fig. 1. Each cantilever has a permanent magnet (PM) attached at the free-end, and an electromagnet (EM) is placed to face PM. Coupling between two cantilevers is caused by the torsional deformation of the coupling rod.

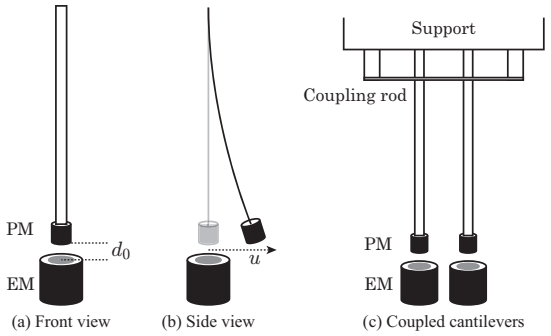

Figure 1: Schematic configuration of a cantilever. (a): Front view. The cylindrical permanent magnet (PM) is attached at the free-end of cantilever. The electromagnet (EM) is placed beneath PM with distance of d_0. (b): Side view. u denotes the tip displacement of cantilever. (c): Two coupled cantilevers.

Due to the Euler-Bernoulli beam theory and the Coulomb's law of magnetic charge, a coupled ordinary differential equation

$$\ddot{u}_n = -\omega_0^2 u_n - C(2u_n - u_{n+1} - u_{n-1}) + \chi \frac{u_n}{\left(u_n^2 + d_0^2\right)^{\frac{3}{2}}} \quad (1)$$

is obtained, where u_n denotes the displacement of the tip of cantilever from the equilibrium position. Natural frequency of a cantilever with PM is ω_0 which is $2\pi \times 35.1\,\mathrm{rad/s}$. Coupling coefficient is represented by C. The third term on the right-hand side of Eq. (1) is contribution of magnetic interaction. The distance between PM and EM when the cantilever is at the rest is denoted by $d_0 = 3.0\,\mathrm{mm}$. The magnitude of the contribution of magnetic force, χ, can be adjusted by the current flowing in EM. In this paper, the conservative system is considered. Then the damping and the external excitation are neglected.

3. Temporally periodic solution

Numerically obtained periodic solutions are shown in Fig. 2. Here, boundaries are fixed, namely, $u_0 = u_3 = 0$.

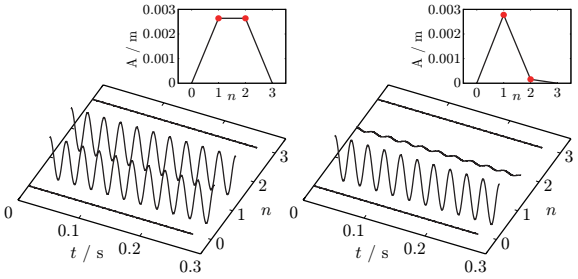

(a) Even mode (b) Odd mode

Figure 2: Wave forms of temporally periodic solutions. The frequency of the solutions is 37 Hz. Parameter setup: $\chi = -2.66 \times 10^{-4}\,\mathrm{m^3/s^2}$, $C = 284\,\mathrm{s^{-2}}$.

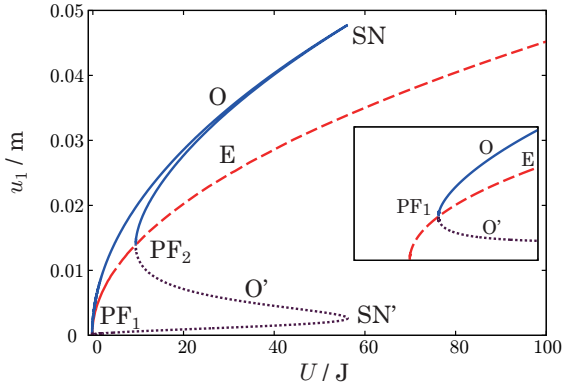

Figure 3: Bifurcation diagram for temporally periodic solutions. Dashed and solid curves indicate even and odd solutions, respectively.

Two kinds of solutions are found, even-mode and odd-mode. For even-mode, both cantilever have the same amplitude as shown in Fig. 2(a). On the other hand, for odd-mode, a cantilever oscillates with large amplitude while the other almost rests around the equilibrium state. Fig. 2(b) shows the wave form of odd-mode.

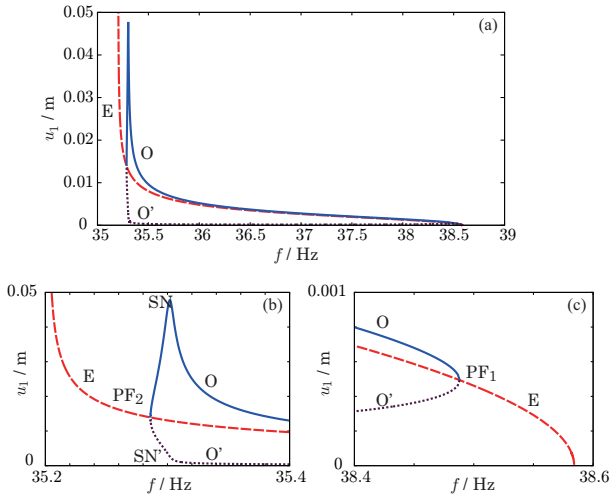

Figure 4: Solutions with respect to their frequency. (a) Overview. (b) Enlargement around the bifurcation point PF_1. (c) Enlargement around the bifurcation point SN and PF_2.

4. Bifurcation set

4.1. Local bifurcations

Since Eq. (1) is a conservative system, the total energy is a bifurcation parameter of the periodic solutions. Fig. 3 shows a bifurcation diagram of even-mode and odd-modes with respect to the total energy of the system. In the figure, O(O') and E correspond to the solution shown in Fig. 2(b) and Fig. 2(a), respectively. As shown in the inset of Fig. 3, stable odd-modes O(O') and an unstable even-mode E appear with the pitch-folk bifurcation (PF_1). As the total energy increases, another pitch-folk bifurcation (PF_2) occurs. At PF_2, the even-mode gains the stability and two unstable odd-modes newly appear. In this regime, five solutions coexist, namely, one stable even-mode and two stable odd-modes, and two unstable odd-modes. The stable and unstable odd-modes disappear through saddle-node bifurcation (SN) at higher energy state. After the saddle-bifurcation occurs, only the stable even-mode remains.

Figure 4 shows the frequency dependence of the amplitude. The frequency of periodic solutions decreases as the amplitude increases, because each cantilever has the soft spring characteristics [6]. As shown in Fig. 4(b), the O-branch has a peak at 35.3 Hz. In fact, the peak corresponds to SN shown in Fig. 3.

4.2. Averaging

The frequency dependence gives the frequency range where stable odd-modes exist. As shown in Fig. 4, the stable odd-modes exist between SN and PF_1. To predict when the bifurcations occur, the averaging method is applied to Eq. (1). $u_n(t)$ is substituted by $A_n \cos \omega t$, and we have,

$$-\omega^2 A_n \cos\omega t = -\omega_0^2 A_n \cos\omega t - C(2A_n - A_{n+1} - A_{n-1})\cos\omega t + \chi \frac{A_n \cos\omega t}{\left(A_n^2 \cos^2\omega t + d_0^2\right)^{\frac{3}{2}}}. \quad (2)$$

Although the last term of the equation contains $\cos\omega t$ in the denominator, the following approximation is applied for simplicity.

$$\chi \frac{A\cos\omega t}{\left\{(A\cos\omega t)^2 + d_0^2\right\}^{\frac{3}{2}}} \to \chi \frac{A\cos\omega t}{\sqrt{\frac{5}{16}A^6 + \frac{9}{8}A^4 d_0^2 + \frac{3}{2}A^2 d_0^4 + d_0^6}}. \quad (3)$$

For the two coupled cantilevers, the following algebraic equation is consequently obtained,

$$\begin{cases} \omega^2 = \omega_0^2 + C\left(2 - \dfrac{a_2}{a_1}\right) - \dfrac{\chi}{d_0^3}\dfrac{1}{\sqrt{\frac{5}{16}a_1^6 + \frac{9}{8}a_1^4 + \frac{3}{2}a_1^2 + 1}}, \\ \omega^2 = \omega_0^2 + C\left(2 - \dfrac{a_1}{a_2}\right) - \dfrac{\chi}{d_0^3}\dfrac{1}{\sqrt{\frac{5}{16}a_2^6 + \frac{9}{8}a_2^4 + \frac{3}{2}a_2^2 + 1}}, \end{cases} \tag{4}$$

where $a_n = A_n/d_0$.

4.3. Bifurcation sets

4.3.1. PF_2

The amplitude of solutions is sufficiently larger than d_0, namely, $a_n \gg 1$. Therefore, the low-order terms in the denominator of the nonlinear term in Eq. (4) are negligible. The highest term of a_n^6 is only considered and we have,

$$\begin{cases} \omega^2 = \omega_0^2 + C\left(2 - \dfrac{a_2}{a_1}\right) - \dfrac{4}{\sqrt{5}}\dfrac{\chi}{d_0^3}\dfrac{1}{a_1^3}, \\ \omega^2 = \omega_0^2 + C\left(2 - \dfrac{a_1}{a_2}\right) - \dfrac{4}{\sqrt{5}}\dfrac{\chi}{d_0^3}\dfrac{1}{a_2^3}. \end{cases} \tag{5}$$

From above equation, a fourth-order polynomial is obtained:

$$\hat{a}^4 + K\hat{a}^3 - \hat{a}^2 - K = 0, \quad K = \frac{4}{\sqrt{5}}\frac{\chi}{Cd_0^3}\frac{1}{a_1^3}, \tag{6}$$

where $\hat{a} = a_2/a_1$. Eq. (6) may have four solutions. One of them is $\hat{a} = 1$ which corresponds to the even-mode. On the other hand, solutions that $\hat{a} \neq 1$ imply odd-modes. Generally, it is difficult to calculate them for the fourth-order polynomial. However, these solutions degenerate to $\hat{a} = 1$ at the bifurcation point PF_2. Therefore, we only focused on when Eq. (6) has the multiple root of $\hat{a} = 1$. By substituting $\hat{a}$ by $1 - \epsilon$ and taking the first-order of ϵ, we have $K = -\dfrac{2}{3}$. Finally, the amplitude and angular frequency of solution at the bifurcation point PF_2 is obtained as follows:

$$A_{PF_2} = A_1 = \left(-\frac{6}{\sqrt{5}}\frac{\chi}{C}\right)^{\frac{1}{3}}, \tag{7}$$

$$\omega_{PF_2}^2 = \omega_0^2 + \frac{5}{3}C. \tag{8}$$

4.3.2. SN

The ratio between amplitude of cantilevers becomes large at the saddle-node bifurcation point SN as shown in Fig. 4. If $\hat{a} = a_2/a_1 \gg 1$, $(2 - a_1/a_2)$ is similarly equal to 2 in Eq. (2). Then, the following polynomial is obtained:

$$W\hat{a}^3 - C\hat{a}^2 + C\hat{a} - W = 0, \quad W = \omega_0^2 + 2C - \omega^2. \tag{9}$$

By factorizing the above equation using the fact that $\hat{a} = 1$ is a root, we have the second-order polynomial $W\hat{a}^2 - (C - W)\hat{a} + W = 0$. In this case, only angular frequency is obtained as:

$$\omega_{SN}^2 = \omega_0^2 + 2C, \tag{10}$$

because $\hat{a}$ is assumed to be infinite.

4.3.3. PF_1

The upper boundary of the frequency range that stable odd-modes exist is the pitch-folk bifurcation point labeled PF_1. At this point, the amplitude of both cantilevers is small with respect to d_0. Then we take Taylor expansion of Eq. (1), and we have

$$\chi\frac{u_n}{\left(u_n^2 + d_0^2\right)^{\frac{3}{2}}} \sim \frac{\chi}{d_0^3}u_n - \frac{3}{2}\frac{\chi}{d_0^5}u_n^3 + \frac{15}{8}\frac{\chi}{d_0^7}u_n^5 + O(u_n^7). \tag{11}$$

Substituting Eq. (11) and $u_n(t) = A_n\cos\omega t$ into Eq. (1) gives

$$\begin{cases} \omega^2 = \left(\omega_0^2 + 2C - \dfrac{\chi}{d_0^3}\right) - C\dfrac{A_2}{A_1} + \dfrac{9\chi}{8d_0^5}A_1^2 - \dfrac{75\chi}{64d_0^7}A_1^4 \\ \omega^2 = \left(\omega_0^2 + 2C - \dfrac{\chi}{d_0^3}\right) - C\dfrac{A_1}{A_2} + \dfrac{9\chi}{8d_0^5}A_2^2 - \dfrac{75\chi}{64d_0^7}A_2^4 \end{cases} \tag{12}$$

From above equation, a fifth-order polynomial of $\hat{a} = A_2/A_1$:

$$\begin{aligned} -C\hat{a} + \frac{9\chi}{8d_0^5}A_1^2 - \frac{75\chi}{64d_0^7}A_1^4 \\ = -C\frac{1}{\hat{a}} + \frac{9\chi}{8d_0^5}A_1^2\hat{a}^2 - \frac{75\chi}{64d_0^7}A_1^4\hat{a}^4. \end{aligned} \tag{13}$$

As the same as the case of PF_2, $\hat{a} = 1$ is a trivial root. Thus the same method is applied to Eq. (13). As a result, a second-order polynomial of A_1^2 is obtained as

$$\frac{1}{2}A_1^4 - \frac{6d_0^2}{25}A_1^2 - \frac{16Cd_0^7}{75\chi} = 0, \tag{14}$$

and finally we have

$$A_{PF_1}^2 = A_1^2 = \frac{6}{25}d_0^2 - \sqrt{\left(\frac{6}{25}d_0^2\right)^2 + \frac{32}{75}C\frac{d_0^7}{\chi}}, \tag{15}$$

$$\omega_{PF_1}^2 = \omega_0^2 + \frac{1}{2}C - \frac{173}{200}\frac{\chi}{d_0^3} - \frac{27}{200}\frac{\chi}{d_0^3}\sqrt{1 + \frac{200d_0^3C}{27\chi}}. \tag{16}$$

4.3.4. Comparison with numerical results

Numerically obtained bifurcation sets are shown in Fig. 5 with the analytical results. In the weak coupling regime, the analytical lines(curve) almost coincide with the numerical curves. In addition, for both analytical and numerical, the frequency range where stable odd-modes exist tends to be narrow as the coupling coefficient becomes large.

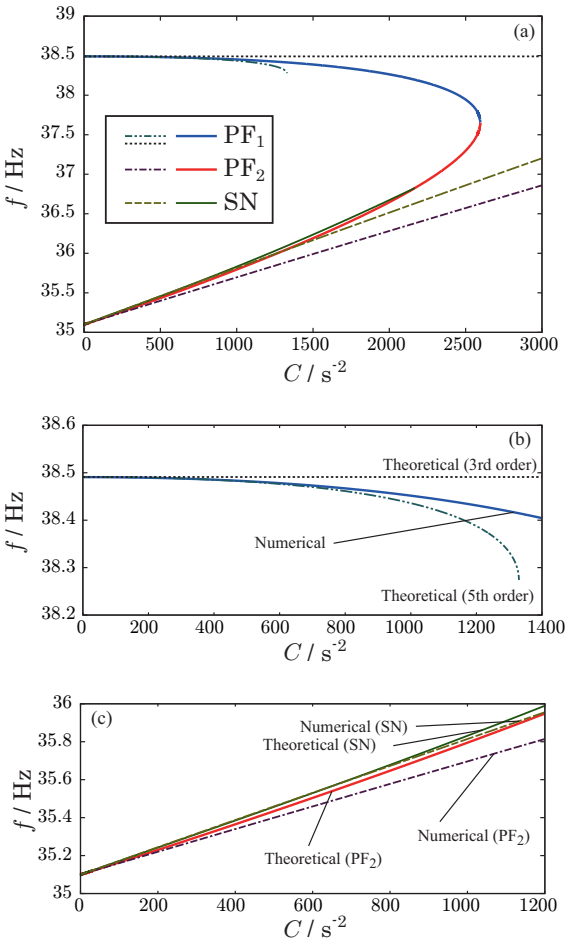

Figure 5: Bifurcation sets for $\chi = -2.66 \times 10^{-4}\,\mathrm{m^3/s^2}$. Solid curve corresponds to numerical results and the other lines and curves are drawn by Eqs. (10), (8), and (16). For PF_1, another result is shown with dotted line which is $\omega'^2_{PF_1} = \omega_0^2 - \dfrac{\chi}{d_0^3}$. This is obtained by considering the first and third terms in the Taylor series of the nonlinear term.

The enlargement of the bifurcation set of PF_1 is shown in Fig. 5(b). For $C < 800\,\mathrm{s^{-2}}$, Eq. (16) is a good approximation. However, around $C = 1300\,\mathrm{s^{-2}}$, the right hand side of Eq. (16) becomes negative. Thus Eq. (16) does not have the real solution for the strong coupling regime. The case that only the first and the third terms of Eq. (11) are taken into account is also shown with the dotted line. Because the analytical solution does not contain the coupling coefficient, the line is parallel to the x-axis.

For PF_2 and SN, the enlargement is shown in Fig. 5(c). As already mentioned before, each analytical line almost coincides with the corresponding numerical curve in the weak coupling regime. However, the error for PF_2 seems to be large even though C is sufficiently small. This implies that the large amplitude approximation is not suitable. In addition, disappearance of the branch for PF_2 and SN is not predicted by the analytical results.

Although the errors between analytical and numerical results tend to be large as the coupling coefficient becomes large, the analytical results give the necessary condition of frequency so that the stable odd-modes exist.

5. Conclusion

In this paper, local bifurcations of periodic solutions in the system of two coupled cantilevers were analytically investigated by using the averaging method and appropriate approximations. As results, the analytical representation of bifurcation sets was obtained. By comparing with numerical results, it was shown that the analytical is valid for the weak coupling regime. Therefore, the analytical results allow us to predict the frequency range where the stable odd-mode exists.

In many degree-of-freedom system, the odd-modes in the two coupled system corresponds to intrinsic localized modes at least in the weak coupling regime because of the anti-continuous limit [7]. Therefore, the results in this paper can be applied to the intrinsic localized modes.

Acknowledgments

This work was supported by the Ministry of Education, Culture, Sports, Science and Technology in Japan, Grant-in-Aid for Young Scientist (B) No. 22760280.

References

[1] A. J. Sievers and S. Takeno, "Intrinsic localized modes in anharmonic crystals," *Phys. Rev. Lett.*, vol.61, p.970, 1988.

[2] S. Flach and A. V. Gorbach, "Discrete breathers – advances in theory and applications," *Phys. Rep.*, vol.467, p.1–116, 2008.

[3] M. Sato, B. E. Hubbard, A. J. Sievers, B. Ilic, D. A. Czaplewski, and H. G. Craighead, "Observation of locked intrinsic localized vibrational modes in a micromechanical oscillator array," *Phys. Rev. Lett.*, vol.90, p.044102, 2003.

[4] M. Sato, B. E. Hubbard, A. J. Sievers, B. Ilic, and H. G. Craighead, "Optical manipulation of intrinsic localized vibrational energy in cantilever arrays," *Europhys. Lett.*, vol.66, (3) p.318, 2004.

[5] M. Kimura and T. Hikihara, "Capture and release of traveling intrinsic localized mode in coupled cantilever array," *Chaos*, vol.19, (1) p.013138, 2009.

[6] M. Kimura and T. Hikihara, "Coupled cantilever array with tunable on-site nonlinearity and observation of localized oscillations," *Phys. Lett. A*, vol.373, (14) p.1257, 2009.

[7] R. S. MacKay and S. Aubry, "Proof of existence of breathers for time-reversible or Hamiltonian networks of weakly coupled oscillators," *Nonlinearity*, vol.7, p.1623, 1994.